ACS APPLIED MATERIALS & INTERFACES

Research Article

www.acsami.org

Herpes Simplex Virus Type-1 Attachment Inhibition by Functionalized Graphene Oxide

Matias Sametband,[†] Inna Kalt,[‡] Aharon Gedanken,*[,†] and Ronit Sarid[‡]

[†]Department of Chemistry, Kanabar Laboratory for Nanomaterials, Institute of Nanotechnology and Advanced Materials, Bar-Ilan University, Ramat Gan 5290002, Israel

[‡]The Mina and Everard Goodman Faculty of Life Sciences, Bar-Ilan University, Ramat-Gan 5290002, Israel

Supporting Information

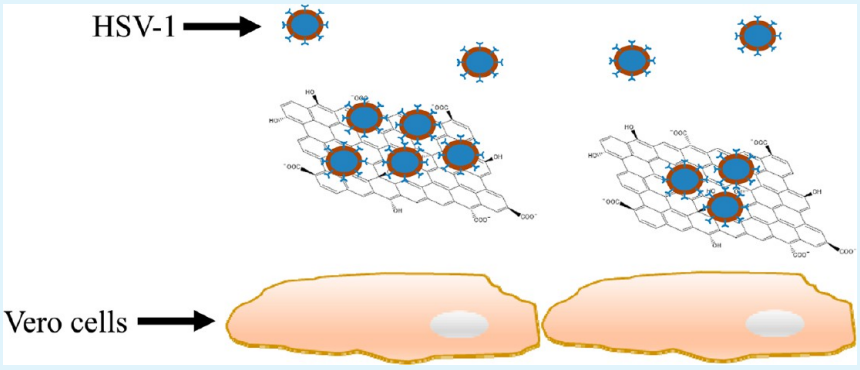

ABSTRACT: Graphene oxide and its derivatives have lately been the subject of increased attention in the field of bioscience and biotechnology. In this article, we report on the use of graphene oxide (GO) derivatives to inhibit herpes simplex virus type-1 (HSV-1) infections, mimicking the cell surface receptor heparan sulfate, and the GO derivatives compete with the latter in binding HSV-1. The inhibition does not affect cell-to-cell spreading. Media content has a significant effect on the inhibition properties of the nanomaterials. These have no cytotoxic effect, suggesting that this is a promising approach for the development of antiviral surfaces and for diagnostic purposes.

KEYWORDS: *herpes simplex virus, graphene oxide, plaque assay reduction, virus inhibition, functionalization*

INTRODUCTION

Herpesviridae is a family of enveloped DNA viruses consisting of eight human herpesviruses (HHVs): herpes simplex virus type 1 and type 2 (HSV-1 and HSV-2, respectively), varicella zoster virus (VZV, HHV-3), Epstein−Barr virus (EBV, HHV-4), cytomegalovirus (CMV, HHV-5), HHV-6, HHV-7, and Kaposi's sarcoma-associated herpesvirus (KSHV, HHV-8).[1]

HSV-1 is a common human pathogen infecting 70−90% of the world population. Humans are the sole natural hosts of HSV-1, and the infections are mostly limited to epithelial cells and neurons of the peripheral nervous system.[2] Viruses of this subfamily establish lifelong infections by entering a non-replicating latent state, thus avoiding host immune response.[3] Primary infection with HSV, as well as reactivation, are associated with oral (HSV-1) and genital (HSV-2) lesions, ocular diseases, and in rare cases encephalitis.[4]

The HSV complex structure consists of a highly ordered protein-shell capsid which encloses the double-stranded 152 kbp linear DNA.[5] The capsid is surrounded by a layer containing more than 20 different viral and host tegument proteins. A host-derived membrane envelope, with about a dozen viral glycoproteins embedded in the lipid bilayer, forms the outer boundary of the viral particle. Five of these glycoproteins (gB, gC, gD, and the complex of gH and gL) mediate the entry of HSV-1 into the host cells.[6]

HSV-1 primary attachment proteins (gB or gC) interact with the host cell by binding to heparan sulfate (HS) proteoglycans.[7] The subsequent step is entry into the cell, which involves binding to a specific entry receptor and is cell-type dependent. Neurons and Vero cells are infected by direct fusion at the plasma membrane and the release of the capsid into the cytosol, while in keratinocytes and HeLa cells entry involves different forms of endocytosis.[8] A broad spectrum of entry receptors, along with a variety of entry mechanisms, enable HSV-1 to infect almost all cell types (including lymphocytes, epithelial cells, fibroblasts, and neurons).

Heparan sulfate (HS) is a negatively charged, linear polymer composed of alternating moieties of hexuronic acid and glucosamine, sulfated at various positions.[9] A large number of proteins interact with HS, mainly through ionic binding, and thereby control different processes in cell development and homeostasis.[10,11] HS has a role in various pathophysiological

Received: November 10, 2013
Accepted: December 23, 2013
Published: December 23, 2013

scenarios, including cancer, amyloid diseases, infectious diseases, inflammatory conditions, and some developmental disorders.[12,13] Virtually all cell types in the body express HS on their surfaces, resulting in a perfect primary receptor for viral infections. Virus binding to HS has relatively low affinity in most cases and serves as a mechanism to increase the virus concentrations on the cell surface, thus facilitating subsequent binding to one or more high-affinity receptors.[14]

The increased attention to graphene and graphene oxide in recent years is the result of their unique physical and chemical properties (high surface area, excellent conductivity, ease of mass production, and the use of standard chemical methods for functionalization).[15] They are broadly used in the fields of electronics,[16] energy storage and conversion,[17] optics,[18] and recently bioscience and biotechnologies.[19] Their high surface area and excellent thermal and electric conductivity were exploited in the development of bio- and immuno-sensors,[20] DNA sensing,[21] biocomposites,[22] gene delivery,[23,24] pathogen sensing at the single-cell level,[25] tissue engineering,[26] transmission electron microscopy (TEM),[27,28] and antibacterial properties.[29] Recently, graphene and graphene oxide have been used for virus detection and research: the graphene oxide (GO)−aptamer complex has been used as a photocatalyst for virus photolysis,[30] the GO-based multiplexed helicase assay was developed for high-throughput screening of inhibitors of HCV NS3 helicase and severe acute respiratory syndrome coronavirus (SARS CoV) helicase,[31] simultaneous detection and knockdown of the hepatitis C virus gene in liver cells,[32] and GO immuno biosensor for virus detection, showing high sensitivity and selectivity.[33]

Multiple simultaneous polyvalent interactions, which collectively increase the strength and selectivity of the interaction as compared to monovalent interactions, play a crucial role in the attachment and entry of most viruses to the cells.[34] Functionalized nanoparticles and micro/nanospheres, bearing a high concentration of surface-bound ligands for multivalent interaction with viruses, were used to inhibit the human immunodeficiency virus (HIV),[35,36] influenza,[37,38] and HSV-1[39] infections with significant success. Applying the same methodology, we introduce herein the use of GO and partially reduced sulfonated GO (rGO−SO_3) for the inhibition of HSV-1 infections through a competitive inhibition mechanism. Both GO and rGO−SO_3 bear multiple negative-charged groups (carboxyl and sulfonate), similarly to HS, thus mimicking the cell's surface. We demonstrate that both nanomaterials inhibit the infection with HSV-1 at nanograms/milliliter concentration levels, through cell attachment inhibition.

EXPERIMENTAL SECTION

GO was synthesized according to an improved Hummer's method.[40] Amounts of 1 g of graphite flakes and 2 g of potassium permanganate were added to 120 mL of 95−97% sulfuric acid and 14 mL of 85% phosphoric acid. After 12 h at 50 °C, the solution was cooled to ambient temperature and immersed in an ice bath, and 130 mL of cold double-distilled water (DDW) was added, followed by 12 mL of 30% hydrogen peroxide. The solution was filtered through a PVDF membrane, and the solid was washed in succession with 30% hydrochloric acid and DDW. The solid was further dispersed in DDW and ultrasonicated for 15 min using a Ti horn from Sonics and Materials VCX 600, 20 kHz, 600 W at 30% efficiency. This was followed by 30 min centrifugation at 4200*g*. The supernatant was dialyzed against DDW for a week and lyophilized, yielding a dark-brown solid. The lyophilized GO was exfoliated by ultrasonication at 30% efficiency, resulting in a brown solution.

Synthesis of partially reduced sulfonated GO (rGO−SO_3)[41] was performed by dispersing 0.075 g of GO in 75 mL of DDW (ultrasonicated for 15 min at 30% efficiency), and the solution's pH was brought to 9−10 using 5% sodium carbonate solution. An amount of 0.6 g of sodium borohydride in 15 mL of DDW was added to the suspension, and the latter was stirred for 1 h at 80 °C. The precipitate was centrifuged and washed repeatedly with DDW. The precipitate was resuspended in 75 mL of DDW, and 10 mL of cold diazonium solution (0.046 g of sulfanilic acid, 0.018 g of sodium nitrite in 10 mL of DDW, and 0.5 mL of 1 M HCl solution) was added to the suspension. The solution was stirred for 2 h, and the temperature was kept below 5 °C. The precipitate was filtered and washed several times with DDW.

Cell cultures were maintained, and plaque reduction assay was performed by Vero African green monkey kidney epithelial cells grown in minimum essential medium (MEM)-Eagle supplemented with 10% heat-inactivated fetal calf serum (FCS), L-glutamine, and penicillin-streptomycin (PS) (Biological Industries, Israel). The cells were maintained at 37 °C under 5% CO_2. For viral infection inhibition experiments, wild-type HSV-1 McIntyre strain and a recombinant HSV-1 strain 17 + 20.5/5, which contains a green fluorescence protein (GFP) expression cassette, were used. Infection inhibition was evaluated by plaque assay. Vero cell cultures (7×10^4 cells/well) were grown in 24-well plates. A 250 μL wild-type HSV-1 McIntyre strain suspension (100 and 1000 plaque-forming units (pfu) per well) was introduced to the cells followed by 1 h incubation in the presence of different GO or rGO−SO_3 concentrations (0−25 μg/mL). Thereafter, the suspension was removed; the cell cultures were washed with growth media; and the cells were overlaid with 750 μL of MEM-Eagle containing 2% FCS and 0.1% human γ globulin (ZLB Behring GmbH, Marburg, Germany). The medium was removed after 48 h, and the cells were stained with 10% Giemsa stain solution. Controls included mock and mock-infected Vero cell monolayers. For multistrain inhibition test and in vitro fluorescent plaque imaging the experiments were conducted in a similar manner with the HSV-1 strain 17 + 20.5/5 (50 and 500 pfu/well), and the plaques were visualized using live imaging fluorescence microscopy (IX81 inverted microscope, Olympus, λ_{ex} = 460−480 nm, λ_{em} = 495−540 nm).

Flow cytometry experiments were conducted by growing 2.8×10^5 Vero cells/well in 6-well plates followed by the addition of 2.4 mL of solution of recombinant HSV-1 strain 17 + 20.5/5 (2×10^5 pfu/well) in the presence of different GO/rGO−SO_3 concentrations (0−20 μg/mL). The cells were collected after 5 h incubation (after one infection cycle), washed with formaldehyde solution and cold 70% ethanol, and repeatedly washed with phosphate buffer saline (PBS). The fluorescence solution was measured by a Beckman Coulter Gallios cell analyzer.

In vitro cytotoxicity and cell cycle assays were performed as follows: Trypan blue toxicity assay was performed by growing Vero cells (7×10^4 cells/well) in the presence of different GO/rGO−SO_3 concentrations (0−50 μg/mL) for 5 days and staining with 10% trypan blue solution. Dead and live cells were counted, and the percent of cell mortality was evaluated. XTT-based colorimetric assay was performed to further validate cell viability after the introduction of GO/rGO−SO_3. The assay was performed according to the manufacturer's protocol (Biological Industries), and the optical density (OD) was measured using a TECAN Spectrafluor Plus (NEOTEC Scientific Instrumentation Ltd.) spectrophotometer at 405 nm wavelength. To validate that the GO/rGO−SO_3 had no effect on cell life cycle, Vero cells (2.8×10^5 Vero cells/well) were grown in a 6-well plate in the presence of GO/rGO−SO_3 (0−50 μg/mL) for 72 h. Cells were harvested, washed with PBS, fixed with cold 70% ethanol, and treated with 0.3 mg/mL of RNase and 0.05 mg/mL of propidium iodide (PI) in PBS containing 0.06% NP-40 for 30 min. Samples were analyzed for DNA content with a Beckman Coulter Gallios flow cytometer. ModFit LT software was used for data analysis.

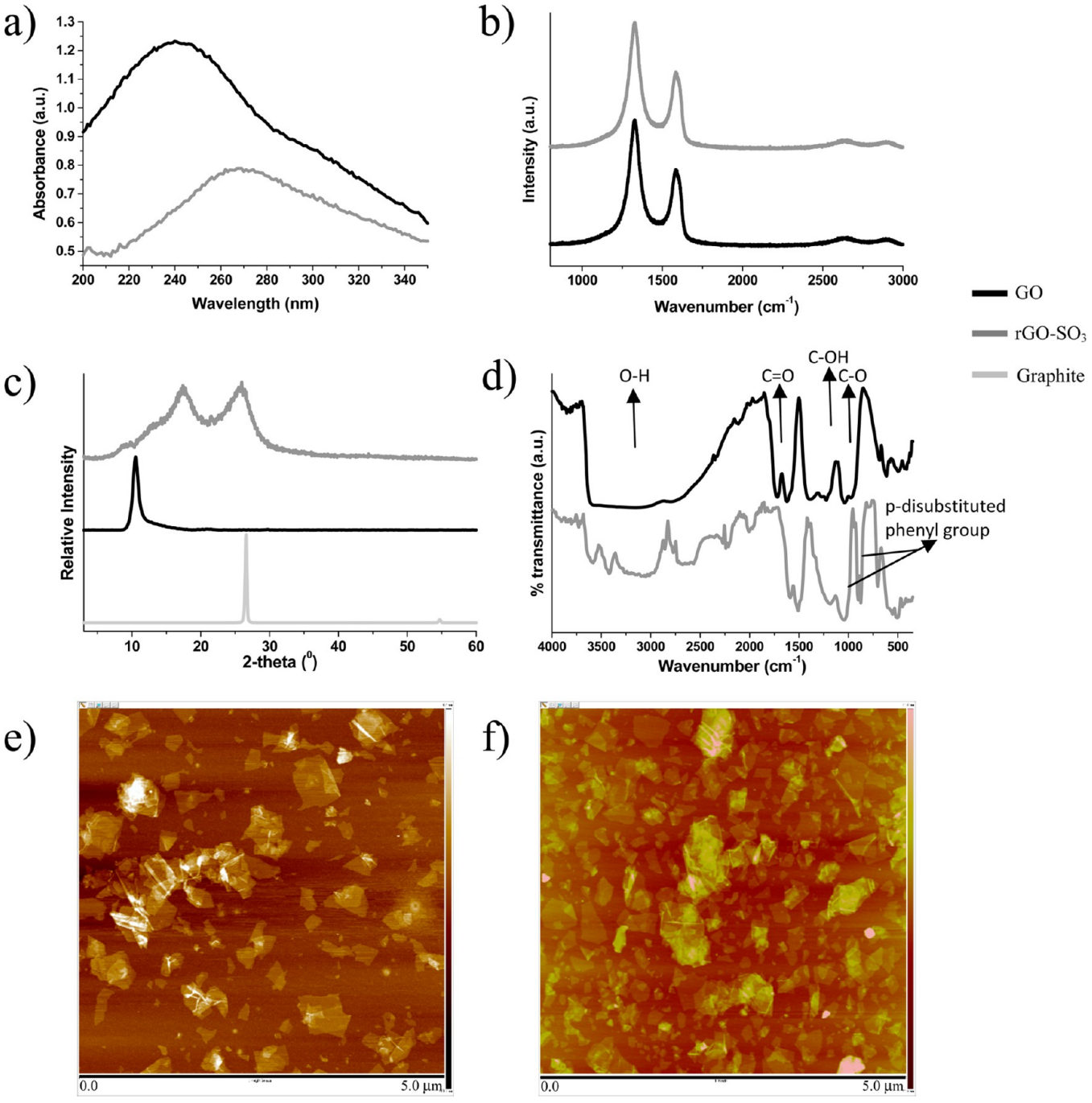

Figure 1. Characterization of GO and rGO−SO_3. (a) UV absorbance of GO and rGO−SO_3 dispersed in DDW. (b) Raman spectra of GO and rGO−SO_3. (c) Pristine graphite, GO, and rGO−SO_3 X-ray diffractions. (d) GO and rGO−SO_3 FTIR spectra. AFM images of GO (e) and rGO−SO_3 (f) (scan dimensions: 5.0 × 5.0 μm).

RESULTS AND DICUSSION

Water-soluble, single-layer GO was synthesized according to an improved Hummer's method.[40] UV−vis absorbance indicated that graphite was oxidized to GO, with an absorption peak at ∼237 nm ($\pi \rightarrow \pi^*$) and a shoulder at ∼300 nm (n $\rightarrow \pi^*$) (Figure 1a), typical of the GO absorption spectrum.[42] Raman spectra showed typical G (∼1590 cm^{-1}) and D (∼1350 cm^{-1}) peaks, indicating an increase of structural defects in the graphitic lattice due to the oxidation process (Figure 1b).[43] The X-ray photoelectron spectroscopy (XPS) C 1s spectra further evidenced the oxidation of the graphite to GO (C═C, 284.8 eV; C−C, 285.4 eV; C−O, 286.9; C═O, 288.7 eV; and O−C═O, 289.8 eV) (Figure S1, Supporting Information).[44] X-ray diffraction (XRD) pattern peaks for pristine graphite and GO (2θ = 26.6° and 2θ = 10.5°, respectively) were measured. These diffraction peaks correspond to previously reported patterns (Figure 1c).[45] Fourier transform infrared (FTIR) spectroscopy showed that oxygen derivatives were present in the sample (O−H groups stretching vibration broad peak at ∼3450 cm^{-1}; C═O stretching vibration peak at 1726 cm^{-1}; C−OH stretching vibration peak at 1226 cm^{-1}; and the C−O stretching peak at 1052 cm^{-1}), further confirming the oxidation of the graphite to GO (Figure 1d).[46] The GO sheets had a ζ potential of −51.1 mV, indicating the presence of negatively

Table 1. Results of Elemental Analysis and XPS Measurements of GO and rGO−SO_3

	elemental analysis					XPS			
	%C	%H	%O	%N	%S	%C	%O	%N	%S
GO	61.83	2.33	34.05	0.01	0.87	63.67	35.50	0.00	0.82
rGO−SO_3	64.52	2.39	23.61	0.19	3.47	67.48	28.49	0.01	3.07

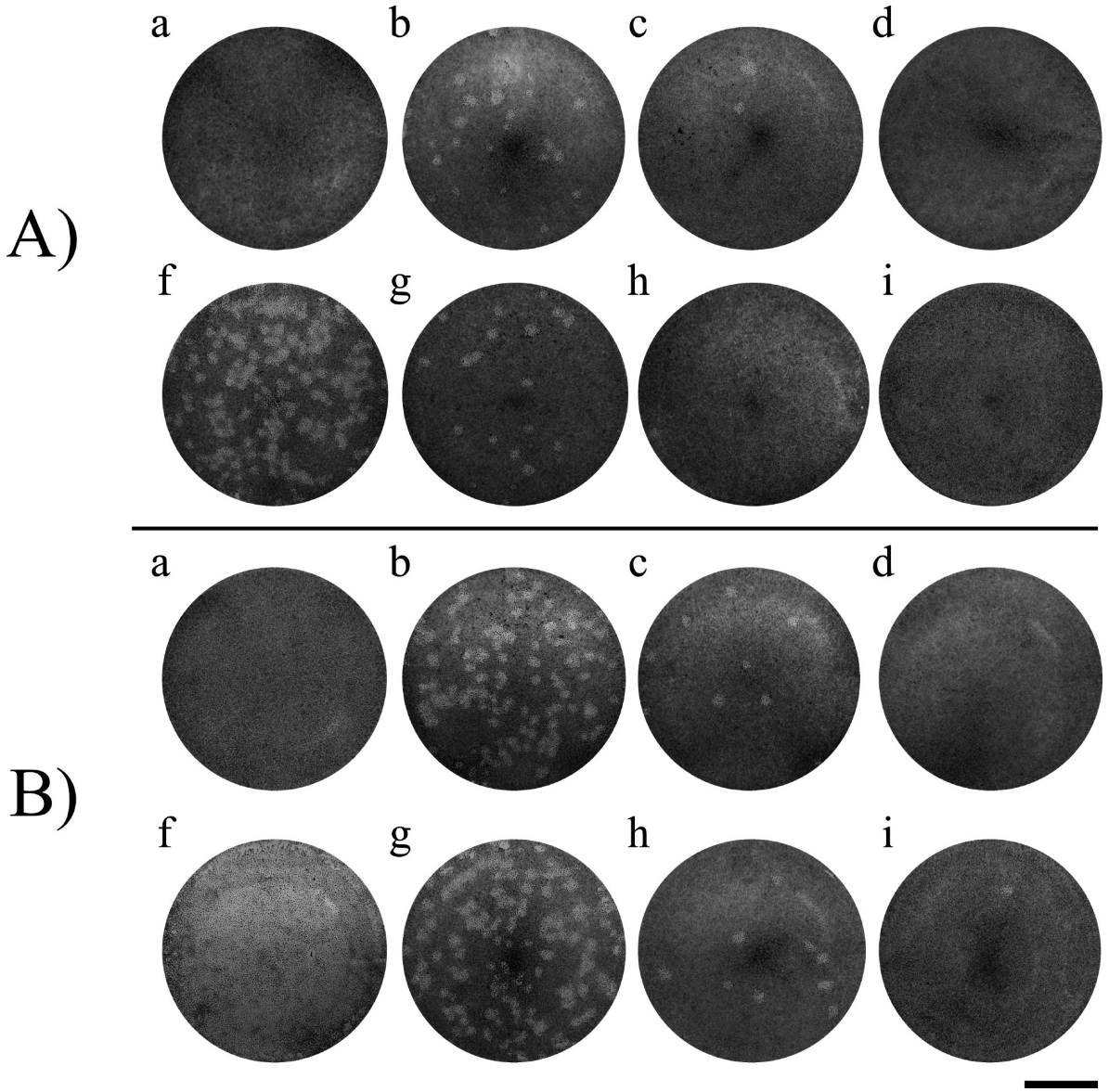

Figure 2. Plaque reduction assay using Vero cell cultures infected by HSV-1 McIntyre strain loads: (A) 100 pfu/well and (B) 1000 pfu/well. (a) Mock noninfected cell cultures; (f) control—cells infected with HSV-1; (b) 0.5, (c) 5, (d) 15 μg/mL of GO and (g) 0.5, (h) 5, and (i) 15 μg/mL of rGO−SO_3 added to the virus suspensions prior to the introduction to the Vero cell cultures. Scale bar: 5 mm. Reduction of infection levels occurred as the concentration of the nanomaterials was increased.

charged groups in the GO structure (Figure S2, Supporting Information). The exfoliated GO sheets had a typical thickness of ∼1.1 nm (Figure S3, Supporting Information), bearing lateral dimensions of several hundred nanometers to a few micrometers, as measured by an atomic force microscope (AFM) (Figure 1, e, scan dimensions of 5.0 × 5.0 μm) and by transmission electron microscopy (TEM) (Figure S4, Supporting Information).

In an attempt to mimic the HS present on the cell's surface enhancing the GO−virus interactions, we introduced a new sulfonate-containing moiety (sulfanilic acid) to the GO.[41] The GO was partially reduced prior to the introduction of the sulfonated groups, to increase the size of sp^2 domains and to consequently facilitate the reaction of the aryl diazonium salt with the partially reduced GO (rGO). The reduction resulted in a red-shift in the absorbance peak to ∼265 nm (Figure 1a).[47,48] The change in D/G intensity ratio in the Raman spectra was minimal (Figure 1b), indicating that the graphitic structure was not significantly altered as would occur upon full GO reduction.[49] A new XRD broad diffraction peak appeared

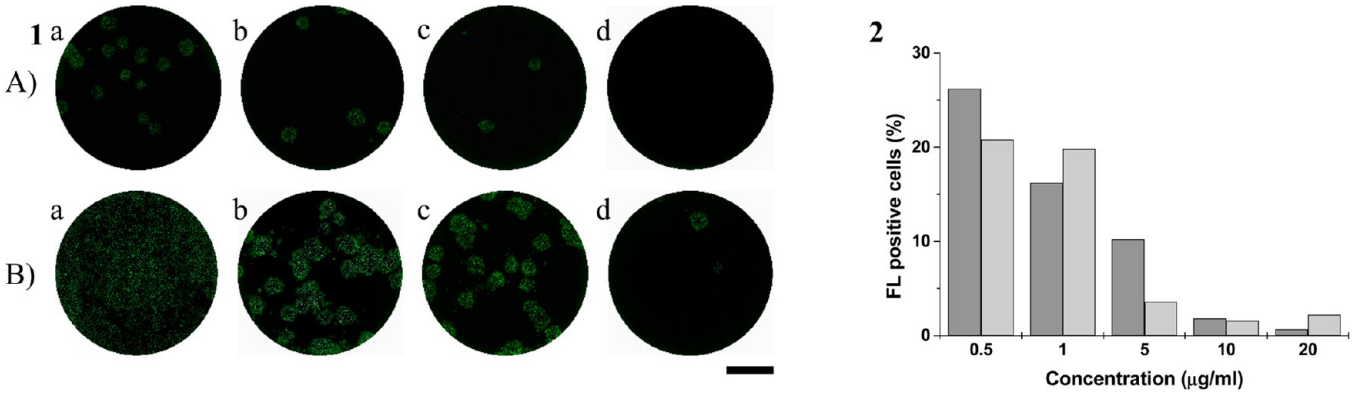

Figure 3. (1) Plaque reduction assay observed by fluorescence microscopy of Vero cell cultures infected with GFP expressing HSV-1 strain 17 + 20.5/5, with loads of (A) 50 pfu/well and (B) 500 pfu/well. (a) Control, w/o the addition of rGO−SO_3; (b) 0.5, (c) 5, and (d) 15 μg/mL of rGO−SO_3 added to the virus suspension prior to the addition to the Vero cell cultures (scale bar: 10 mm). (2) Flow cytometry of Vero cells infected with GFP expressing HSV-1 in the presence of different GO (grey) and rGO−SO_3 (light grey) concentrations. Cells were collected at 5 h post infection. Shown are the percentages of GFP positive infected Vero cells out of the total cell population. It was clear that the number of plaques visualized decreased as the concentration of rGO−SO_3 was increased. The total number of fluorescent cells also decreased, indicating on effective infection inhibition by the nanomaterial.

located in between the GO and pristine graphite peaks, corresponding to changes in interlayer distances and a partial removal of oxide groups, further indicating partial reduction of the graphite (Figure 1c). C 1s XPS spectra showed that the C−O, C═O, and O−C−O peaks were weakened after the partial reduction (Figure S1, Supporting Information). Thereafter, the diazonium salt was introduced to the rGO. The presence of sulfonated groups was confirmed by elemental analysis and XPS, which indicated an average of ∼3.5% sulfur content in the samples (Table 1). A low percentage of sulfur was present in the GO, originating from the use of sulfuric acid during the oxidation process of graphite. We measured the S 2p XPS spectra of the sulfonated rGO (rGO−SO_3) and found a maximum binding energy (BE) peak at 168.3 eV, corresponding to the sulfonate group (Figure S5, Supporting Information).[50] Changes in the FTIR spectrum further indicated the partial removal of oxygen-containing groups and the presence of the sulfonate and the phenyl group (characteristic vibrations of a p-disubstituted phenyl group at ∼1007 cm^{-1} (C−H in-plane bending) and ∼830 cm^{-1} (out-of-plane hydrogen wagging)) (Figure 1b).[35] The rGO−SO_3 ζ potential was slightly more negative (−53.1 mV) than the GO potential, indicating that the charge density on both nanomaterials was similar (Figure S2, Supporting Information). The rGO−SO_3 thickness was similar to that of the GO at ∼1.1 nm, as measured by AFM (Figure S3, Supporting Information). No noticeable difference in the rGO−SO_3 morphology and dimensions was noticed compared to GO when imaged by TEM and high-resolution scanning electron microscopy (HR-SEM) (Figure S4, Supporting Information).

We performed a plaque reduction assay to evaluate the antiviral properties of GO and rGO−SO_3. This assay is typically used to quantitate the infectious virus by assessing the plaque forming units (pfu's) in a given sample. In this assay, cell monolayers are infected with a low ratio of virus, resulting in a sporadic cell infection. The spreading of the virus is limited by the presence of antibodies in the media, so the virus spreading is limited to adjacent cells after lysis of the infected cells. After several infection cycles a local destruction area is created, called plaque, which is representative of one infectious viral unit. The number of plaques formed is counted, representing the total infective units in the sample, and the viral titer is determined (pfu/mL) for a given virus stock. The experiments were conducted by introducing HSV-1 McIntyre strain loads (100 and 1000 pfu per well) to Vero cell cultures grown in 24-well plates, in the presence of different GO or rGO−SO_3 concentrations (0−25 μg/mL). The plaques, formed by the presence of human γ globulin, which inactivates viruses released to the media, were evaluated after 48 h from initial infection. The cell cultures had a typical cytopathic effect in the absence of the nanomaterials, and a high number of plaques were formed in the control sample for the lower virus titer (average of 132 plaques/well). Massive cell distraction was observed in the case of the higher viral titer, indicating a high level of viral infection (Figure 2A and 2B, f, respectively). As the concentration of both materials increased in the suspension, partial inhibition of plaque formation occurred, up to total infection blocking at 5 μg/mL for the low virus titer (Figure 2A, d,i) and 15 μg/mL for the high virus titer (Figure 2B, d,i). Inhibition activity was noticed at concentration as low as 125 ng/mL (Figure S6, Supporting Information). No noticeable plaque-size difference was observed when comparing plaques formed in the presence or in the absence of both materials, suggesting that the nanomaterials did not affect virus infection through cell-to-cell spreading. Sulfonate groups were introduced to the GO in an attempt to enhance the GO viral inhibition properties. In contrast to our expectations, no noticeable differences in inhibition activity were noticed between GO and rGO−SO_3 (Figure 2, b−d and g−i, respectively). Both materials had roughly the same ζ potential (−51.1 and −53.1 mV for GO and rGO−SO_3, respectively) which may be an indication that the charge group identity has a lesser effect on the inhibition activity than the charge density. This is in contrast to our previous findings, when functionalized gold nanoparticles were used to inhibit viral infection, and the identity of the functional group had an effect on the inhibition properties of the nanoparticles.[51] The reason for this discrepancy is unknown, though the density and spatial organization of the functional groups as well as the size and other physical properties of the particles could account for this difference. In addition, rGO−SO_3 larger hydrophobic domains had no effect on the nanomaterial's inhibitory properties,

suggesting the importance of the charge density on the interaction with the virus.

To further investigate the multistrain antiviral activity of the GO and rGO−SO_3, a recombinant HSV-1 strain 17 + 20.5/5, which contains a green fluorescence protein (GFP) expression cassette, was used. The viruses express GFP during the infection cycle, allowing for the visualization of the virus spreading in the cell cultures by fluorescence microscopy. In addition, cell sorting and counting the number of infected cells can be assessed by flow cytomerty. Experiments similar to those described above were performed, using two viral titers (50 and 500 pfu/well). In agreement with the results of previous experiments, as the concentration of the GO/rGO−SO_3 increased, a higher inhibition activity was found (Figure 3, 1). No plaque formation occurred at 5 μg/mL at the lower virus titer, while at higher titer levels only a small number of plaques were generated. This suggested that the inhibition properties of both nanomaterials were not strain dependent.

We performed flow cytometry measurements of Vero cells infected with the GFP expressing viral strain to quantify the proportion of infected Vero cells out of the total cell population in the presence of GO or rGO−SO_3. The cell cultures were grown in a 6-well plate (2.8×10^5 cells/well) and infected with HSV-1 GFP-expressing strain (2×10^5 pfu/well), to achieve high infection levels. The cells were collected 5 h after infection, allowing for a single infection cycle, and the number of cells primarily infected by the viruses was counted, in the presence of different GO/rGO−SO_3 concentrations (0−20 μg/mL). The experiments were conducted in the absence of γ globulin to reduce any external interventions to the interaction between the viruses and the nanomaterials. The fluorescent cells were analyzed using a Beckman Coulter Gallios cell analyzer, and the results indicated a reduction of the infected cell percentage from ∼25% infected cells in the control down to 2−4% out of the total cell population for 10 μg/mL of GO/rGO−SO_3 (Figure 3, 2). As noticed previously, no significant difference was observed between the nanomaterial inhibition efficiency. Both nanomaterials are very efficient at reducing viral infections, and a competitive attachment inhibition mechanism is believed to be the explanation for these results.

Since no noticeable plaque-size difference was observed when comparing between plaques formed in the presence or in the absence of both materials, we hypothesized that our compounds did not affect virus infection through cell-to-cell spreading. To test this hypothesis, Vero cell cultures were infected with the HSV-1 McIntyre strain (100 pfu/well) for 1 h, washed, and overlaid with media containing γ globulin. This process allowed the attachment of the viruses to the cells, enabling primary viral infection while removing unattached viruses. Infection spreading thus occurs solely through cell-to-cell infection due to the presence of γ globulin, which inactivates viruses released to the media. Addition of different concentrations of either GO or rGO−SO_3 (0−20 μg/mL) in combination with γ globulin allowed us to study the effect these nanomaterials had on cell-to-cell spread infections. The number of plaques formed in the presence of GO or rGO−SO_3 was similar to the control, and no inhibition of infection resulted from the addition of the nanomaterials (Figure S7, Supporting Information). Changes in plaque morphology and diameter were not noticed when comparing the control to the treated samples, in agreement with previous findings. We believe that GO and rGO−SO_3 must penetrate the intercellular region between the cells to effectively inhibit cell-to-cell spreading. Even though these nanomaterials have a width of ∼1.1 nm, their lateral size varies from several hundred nanometers up to a few micrometers, which may prevent them from entering the intercellular region. The inability to inhibit viral infections through cell-to-cell inhibition infers that the main inhibition mechanism is through attachment blocking.

To further examine the attachment inhibition effect, time-dependent inhibition was tested by pre-incubating the viruses (1000 pfu/well) and the nanomaterials (1 μg/mL) for different time intervals (0−60 min) before they were introduced to the cell cultures. Interestingly, the inhibition efficiency increased as the pre-incubation period was prolonged up to 20 min (Figure S8, Supporting Information), and no difference in plaque formation was noticed for longer incubation intervals.

It was previously described that growth media content interacts with the GO's basal plane, masks the charges present on the GO, and reduces its stability in the solution.[52] We tested the effect of the growth media content on the inhibition efficiency of the nanomaterials by suspending the GO and rGO−SO_3 (0−5 μg/mL) in growth media for 1 h, followed by overlaying the suspensions on the cell cultures and introducing the virus suspensions (100 pfu/well) without the removal of the nanomaterials. After 1 h incubation the suspension was removed, and fresh growth media with γ globulin was added. After 48 h it was observed that no inhibition of virus infections occurred, and the number of plaques formed in the control and the treated samples was similar, indicating that the nanomaterials lost their antiviral activity after 1 h incubation in growth media (Figure S9A, Supporting Information). To test whether the antiviral activity degradation was time dependent, the GO and rGO−SO_3 were dispersed in growth media at a concentration of 5 μg/mL, and the viruses were added to these suspensions at different incubation time points. The nanomaterial−virus suspensions were introduced to the cell cultures, and the experiments were continued similarly as before. No loss of antiviral activity was noticed when the viruses were added immediately after the nanomaterials were dispersed in growth media (Figure S9B, b, Supporting Information). In contrast, as the nanomaterial incubation time in the growth media was prolonged, a higher number of plaques were formed, and the antiviral activity was reduced (Figure S9B, c−f, Supporting Information). It was noticed that after 60 min the nanomaterials lost almost all their antiviral activity. When similar experiments were conducted in PBS ×1, this effect was not as noticeable, and the nanomaterial efficiency was not hampered (Figure S9c, Supporting Information). This suggests that the growth media content interacted with GO/rGO−SO_3 through electrostatic and hydrophilic−hydrophobic interactions, resulting in a reduction in their inhibitory properties. We believe that growth media content masks the negative charges present on the nanomaterials, lowering their stability in the dispersion and reducing their interaction with the viruses. It may also be that cell-to-cell inhibition is not occurring due to the loss of the nanomaterial stability and the reduction in the inhibition properties in growth media and not just due to the inability to enter the intercellular region due to the nanomaterial size.

We performed three independent cytotoxicity tests to verify that GO/rGO−SO_3 had no toxic effect towards the Vero cells. Trypan blue assay was applied for testing the cytoxicity levels of GO and rGO−SO_3 on Vero cells at a concentration of 0−50 μg/mL and compared to nanomaterial-free cell culture (control). Cell viability was assessed after 5 days. No significant

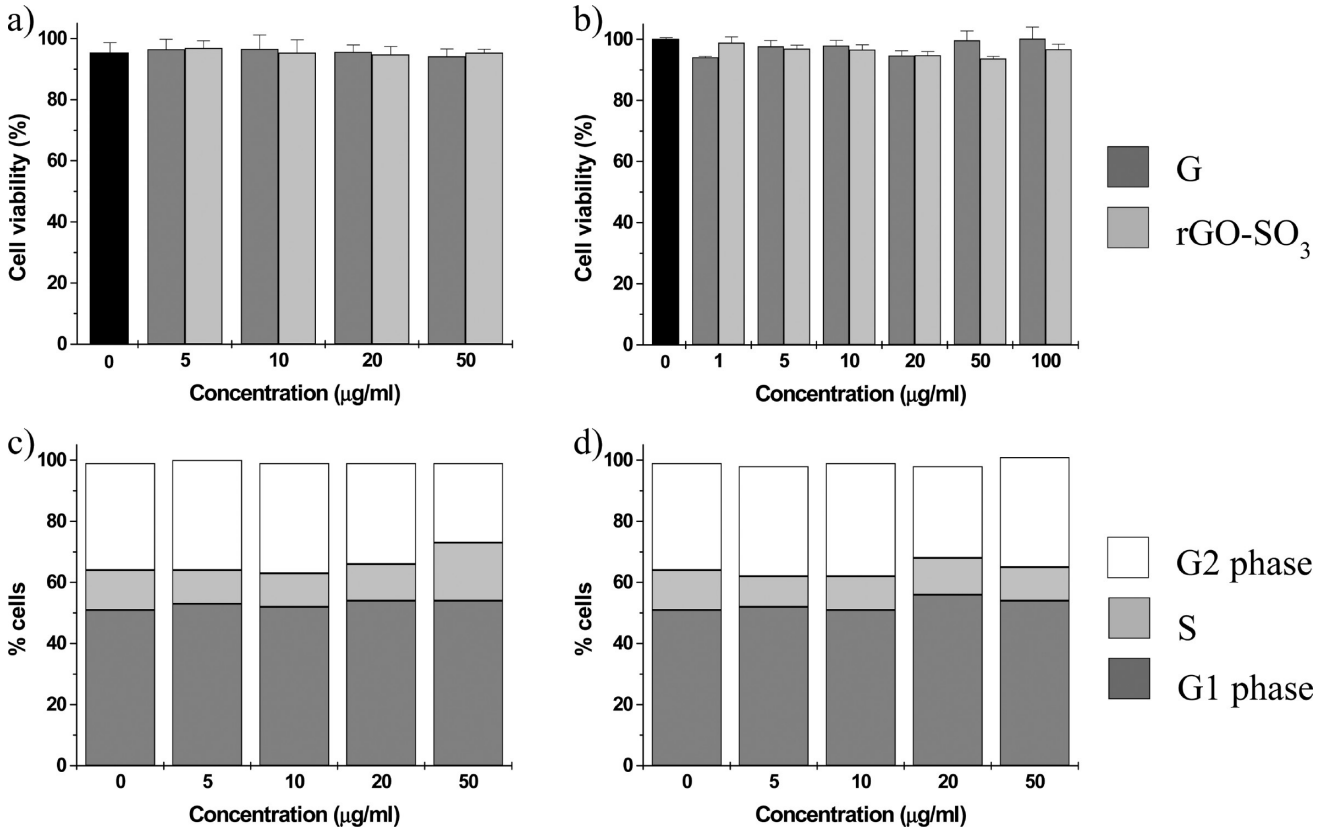

Figure 4. Cytotoxicity assays: (a) Trypan blue cytotoxicity assay; (b) XTT enzyme-based assay; Flow cytometry of GO and rGO−SO_3 (c and d, respectively) treated Vero cell cultures. GO and rGO−SO_3 showed no toxic effect towards the cell cultures and did not affect the cells' life cycle.

difference in cell mortality between the treated cultures and the control was found (Figure 4A). We further tested the cytotoxic effect of GO/rGO−SO_3 by an enzyme-based method using the XTT assay. Similarly to previous results, no cytotoxic effect was noticed at concentrations up to 100 μg/mL (Figure 4B). Cell cycle analysis was performed using the propidium iodide (PI) DNA staining protocol to verify that the nanomaterials did not affect the cell's life cycle. Cell cultures were incubated with GO or rGO−SO_3 (0−50 μg/mL) for 72 h before they were collected, washed, fixed, and stained. This was followed by analysis by flow cytometry. The cell cycle was not affected by the presence of the nanomaterials during the period tested (Figure 4C and 4D), with minor differences in cell phase distribution in the samples. The latter are attributed to normal deviations that are not related to the presence of the nanomaterials. MTT and XTT methods may provide false negative results when they are used to assess carbon-based material's toxicity.[53] Taken together with the Trypan blue and cell cycle analysis we can conclude that in our case the nanomaterials showed no cytotoxicity, and there was no increase in cell mortally nor changes in the cells life cycle. This conclusion coincides with previous reports, although debate still exists whether GO is toxic to cells.[54,55]

CONCLUSION

In conclusion, we demonstrated using a plaque reduction assay that GO and rGO−SO_3 blocked HSV-1 infections (HSV-1 McIntyre strain, as well as 17 + 20.5/5 HSV-1) at relatively low concentrations. We showed a reduction in plaque formation and a drop in GFP positive cells in the presence of both GO and rGO−SO_3. Even though we expected the presence of sulfonate groups on the basal plane of the GO to increase the inhibitory efficiency, no noticeable differences in inhibition activity occurred when rGO−SO_3 was tested. Both materials have roughly the same ζ potential, indicating that the charge density is probably the dominant factor affecting the inhibition properties of our compounds. We believe that viral attachment blocking was the main inhibition mechanism, and cell-to-cell spread is not affected by the presence of the nanomaterials. We presume that due to the large lateral dimension of hundreds of nanometers the nanomaterials are not able to penetrate into the intercellular region and inhibit the spreading. Growth media content alters the GO/rGO−SO_3 antiviral properties, and the latter, as well as solubility, were found to decrease with time. Three independent cytotoxicity tests showed that the nanomaterials had no toxicity effect toward the Vero cell cultures, indicating that these materials can be applied for cell culture experiments. GO and its derivatives will allow us to develop new methods to inhibit and detect viral infections. Using the GO derivatives' intrinsic properties (conductive, optical, and polyvalency) will enable the development of antiviral surfaces and of detection devices which react to viral presence.

ASSOCIATED CONTENT

Supporting Information

Additional experimental information; GO and rGO−SO_3 characterization; low nanomaterial concentrations, cell-to-cell inhibition, time-dependent inhibition, and media effect on inhibition. This material is available free of charge via the Internet at http://pubs.acs.org.

AUTHOR INFORMATION

Corresponding Author

*Tel.: +972 3 5318315. Fax: +972 3 7384053. E-mail: gedanken@mail.biu.ac.il.

Notes

The authors declare no competing financial interest.

REFERENCES

(1) Jackson, J. O.; Jardetzky, T. S.; Longnecker, R. *Nat. Rev. Microbiol.* **2011**, *9*, 369.
(2) Liashkovicha, I.; Hafezib, W.; Kunb, J. M.; Oberleithnera, H.; Shahina, V. *J. Mol. Recognit.* **2011**, *24*, 414.
(3) Nicoll, M. P.; Proença, J. T.; Efstathiou, S. *FEMS Microbiol. Rev.* **2012**, *36*, 684.
(4) Hadigal, S.; Shukla, D. *Viruses* **2013**, *5*, 1447.
(5) McGeoch, D. J.; Rixon, F. J.; Davison, A. J. *Virus Res.* **2006**, *117*, 90.
(6) Subramanian, R. P.; Geraghty, R. J. *Proc. Natl. Acad. Sci. U.S.A.* **2007**, *104*, 2903.
(7) Choudhary, S.; Marquez, M.; Alencastro, F.; Spors, F.; Zhao, Y.; Tiwari, V. *J. Biomed. Biotechnol.* **2011**, *2011*, 264350.
(8) Karasneh, G. A.; Shukla, D. *Virol. J.* **2011**, *8*, 481.
(9) Bishop, J. R.; Schuksz, M.; Esko, J. D. *Nature* **2007**, *446*, 1030.
(10) Lindahl, U.; Li, J. P. *Int. Rev. Cell Mol. Biol.* **2009**, *276*, 105.
(11) Bernfield, M.; Gotte, M.; Park, P.W. *Annu. Rev. Biochem.* **1999**, *68*, 729.
(12) Lindahl, U.; Kjellen, L. *J. Int. Med. Res.* **2013**, *273*, 555.
(13) Park, P. J.; Shukla, D. *Exp. Eye Res.* **2013**, *110*, 1.
(14) Zhu, W.; Yang, L. J.; Liang, G. D. *Biomed. Environ. Sci.* **2011**, *24*, 81.
(15) Singha, V.; Jounga, D.; Zhaia, L.; Dasa, S.; Khondakera, S. I.; Seal, S. *Prog. Mater. Sci.* **2011**, *56*, 1178.
(16) Sun, D. M.; Liu, C.; Ren, W. C.; Cheng, H. M. *Small* **2013**, *9*, 1188.
(17) He, Y.; Chen, W.; Gao, C.; Zhou, J.; Li, X.; Xie, E. *Nanoscale* **2013**, *5*, 8799.
(18) Jariwala, D.; Sangwan, V. K.; Lauhon, L. J.; Marks, T. J.; Hersam, M. C. *Chem. Soc. Rev.* **2013**, *42*, 2824.
(19) Feng, L. Y.; Wu, L.; Qu, X. G. *Adv. Mater.* **2013**, *25*, 168.
(20) Liu, N.; Chen, X.; Mab, Z. *Biosens. Bioelectron.* **2013**, *48*, 33.
(21) Bi, S.; Zhao, T.; Luo, B. *Chem. Commun.* **2012**, *48*, 106.
(22) Hua, Y.; Li, F.; Han, D.; Wu, T.; Zhang, Q.; Niu, L.; Bao, Y. *Anal. Chim. Acta* **2012**, *753*, 82.
(23) Zhou, X.; Laroche, F.; Lamers, G. E. M.; Torraca, V.; Voskamp, P.; Lu, T.; Chu, F.; Spaink, H. P.; Abrahams, J. P.; Liu, Z. *Nano Res.* **2012**, *5*, 703.
(24) Han, T. H.; Lee, W. J.; Lee, D. H.; Kim, J. E.; Choi, E. Y.; Kim, S. O. *Adv. Mater.* **2010**, *22*, 2060.
(25) Ang, P. K.; Li, A.; Jaiswal, M.; Wang, Y.; Hou, H. W.; Thong, J. T.; Lim, C.T.; Loh, K. P. *Nano Lett.* **2011**, *11*, 5240.
(26) Lee, S. K.; Kim, H.; Shim, B. S. *Carbon* **2013**, *14*, 63.
(27) Jeon, J.; Lodge, M. S.; Dawson, B. D.; Ishigami, M.; Shewmaker, F.; Chen, B. *Biochim. Biophys. Acta* **2013**, *1830*, 3807.
(28) Nair, R. R.; Blake, P.; Blake, J. R.; Zan, R.; Anissimova, S.; Bangert, U.; Golovanov, A. P.; Morozov, S. V.; Geim, A. K.; Novoselov, K. S.; Latychevskaia, T. *Appl. Phys. Lett.* **2010**, *97*, 153102.
(29) Liu, S.; Zeng, T. H.; Hofmann, M.; Burcombe, E.; Wei, J.; Jiang, R.; Kong, J.; Chen, Y. *ACS Nano* **2011**, *5*, 6971.
(30) Hu, X.; Mu, L.; Wen, J.; Zhou, Q. *Carbon* **2012**, *50*, 2772.
(31) Jang, H.; Ryoo, S. R.; Kim, Y. K.; Yoon, S.; Kim, H.; Han, S. W.; Choi, B. S.; Kim, D. E.; Min, D. H. *Angew. Chem., Int. Ed.* **2013**, *52*, 2340.
(32) Kim, S.; Ryoo, S. R.; Na, H. K.; Kim, Y. K.; Choi, B. S.; Lee, Y.; Kim, D. E.; Min, D. H. *Chem. Commun.* **2013**, *49*, 8241.
(33) Jung, J. H.; Cheon, D. S.; Liu, F.; Lee, K. B.; Seo, T. S. *Angew. Chem., Int. Ed.* **2010**, *49*, 5708.
(34) Mammen, M.; Choi, S. K.; Whitesides, G. M. *Angew. Chem., Int. Ed.* **1998**, *37*, 2754.
(35) Gianvincenzo, P. D.; Marradi, M.; Martinez-Avila, O. M.; Bedoya, L. M.; Alcami, J.; Penades, S. *Bioorg. Med. Chem. Lett.* **2010**, *20*, 2718.
(36) Martinez-Vila, O.; Bedoya, L. M.; Marradi, M.; Clavel, C.; Alcami, J.; Penades, S. *ChemBioChem* **2009**, *10*, 1806.
(37) Stanley, M.; Cattle, N.; McCauley, J.; Martin, S. R.; Rashid, A.; Field, R. A.; Carbaina, B.; Streicher, H. *MedChemComm* **2012**, *3*, 1373.
(38) Papp, I.; Sieben, C.; Ludwig, K.; Roskamp, M.; Bottcher, C.; Schlecht, S.; Herrmann, A.; Haag, R. *Small* **2010**, *6*, 2900.
(39) Baram-Pinto, D.; Shukla, S.; Gedanken, A.; Sarid, R. *Small* **2010**, *6*, 1044.
(40) Marcano, D. C.; Kosynkin, D. V.; Berlin, J. M.; Sinitskii, A.; Sun, Z.; Slesarev, A.; Alemany, L. B.; Lu, W.; Tour, J. M. *ACS Nano* **2010**, *4*, 4806.
(41) Si, Y.; Samulski, E. T. *Nano Lett.* **2008**, *8*, 1679.
(42) Zhang, J.; Yang, H.; Shen, G.; Cheng, P.; Zhang, J.; Guo, S. *Chem. Commun.* **2010**, *46*, 1112.
(43) Jiang, Xu.; Ma, Y.; Li, J.; Fan, Q.; Huang, W. *J. Phys. Chem. C* **2010**, *114*, 22462.
(44) Park, S.; Bielawski, C. W.; Ruoff, R. S. *Chem. Soc. Rev.* **2010**, *39*, 228.
(45) He, H.; Gao, C. *Chem. Mater.* **2010**, *22*, 5054.
(46) Paredes, J. I.; Villar-Rodil, S.; Martinez-Alonso, A.; Tascon, J. M. D. *Langmuir* **2008**, *24*, 10560.
(47) Luo, D.; Zhang, G.; Liu, J.; Sun, X. *J. Phys. Chem. C* **2011**, *115*, 11327.
(48) Zhou, X.; Zhang, J.; Wu, H.; Yang, H.; Zhang, J.; Guo, S. *J. Phys. Chem. C* **2011**, *115*, 11957.
(49) Zhu, Y.; Tour, J. M. *Nano Lett.* **2010**, *10*, 4356.
(50) Choi, B. G.; Park, H. S.; Yang, M. H.; Jung, Y. M.; Lee, S. Y.; Hong, W. H.; Park, T. J. *Nanoscale* **2010**, *2*, 2692.
(51) Sametband, M.; Shukla, S.; Meningher, T.; Hirsh, S.; Mendelson, E.; Sarid, R.; Gedanken, A.; Mandelboim, M. *MedChemComm* **2011**, *2*, 421.
(52) Hong, B. J.; Compton, O. C.; An, Z.; Eryazici, I.; Nguyen, S.T. *ACS Nano* **2012**, *24*, 63.
(53) Liao, K. H.; Lin, Y. S.; Macosko, C. W.; Haynes, C. L. *ACS Appl. Mater. Interfaces* **2011**, *3*, 2607.
(54) Schinwald, A.; Murphy, F.A.; Jones, A.; MacNee, W.; Donaldson, K. *ACS Nano* **2012**, *24* (6), 736.
(55) Wang, K.; Ruan, J.; Song, H.; Zhang, J.; Wo, Y.; Guo, S.; Cui, D. *Nanoscale Res. Lett.* **2011**, *6*, 8.